Applied Surface Science 259 (2012) 399–405

Contents lists available at SciVerse ScienceDirect

Applied Surface Science

journal homepage: www.elsevier.com/locate/apsusc

Comparative study of the ZnO and $Zn_{1-x}Cd_xO$ nanorod emitters hydrothermally synthesized and electrodeposited on *p*-GaN

O. Lupan[a,b,c,*], T. Pauporté[b,**], L. Chow[a], G. Chai[a], B. Viana[d], V.V. Ursaki[e], E. Monaico[c,e], I.M. Tiginyanu[e]

[a] Department of Physics, University of Central Florida, PO Box 162385 Orlando, FL 32816-2385, USA
[b] Laboratoire d'Electrochimie, Chimie des Interfaces et Modélisation pour l'Energie (LECIME) UMR-7575, ENSCP-Chimie Paristech, 11 rue Pierre et Marie Curie, 75231 Paris, cedex 05, France
[c] Department of Microelectronics and Semiconductor Devices, Technical University of Moldova, 168 Stefan cel Mare Blvd., MD-2004, Chisinau, Republic of Moldova
[d] Laboratoire de Chimie de la Matière Condensée de Paris, UMR 7574, ENSCP, 11 rue P. et M. Curie, 75231 Paris cedex 05, France
[e] Institute of Electronic Engineering and Nanotechnologies, Institute of Applied Physics, Academy of Sciences of Moldova, MD-2028 Chisinau, Republic of Moldova

ARTICLE INFO

Article history:
Received 17 March 2012
Received in revised form 11 July 2012
Accepted 13 July 2012
Available online 20 July 2012

Keywords:
ZnO Nanorods
Hydrothermal growth
Electrochemical deposition
Epitaxy
Photoluminescence
UV-light emitting diode
LED
ZnO/*p*-GaN heterojunction

ABSTRACT

Hydrothermal synthesis and electrodeposition are low-temperature and cost-effective growth techniques of high quality nanostructured active materials for opto-electronic devices. Here we report a hydrothermal seed layer-free and rapid synthesis (15 min) of epitaxial nanorod arrays of ZnO on *p*-GaN(0 0 0 1). The effects of hydrothermal (HT) versus electrochemical deposition (ECD) synthesis on the optical properties of ZnO nanorods/nanowires on *p*-GaN substrate are compared in details. For both types of layers, a strong photoluminescent UV-emission was found indicating the high quality of the synthesized ZnO layer. The hetero-structures were used for LED applications. With HT-ZnO and ECD-ZnO, UV-emission started at remarkably low forward voltage of 3.9–4.0 V and 4.4 V respectively and increased rapidly. Moreover, the LED structures showed a stable and repeatable electroluminescence. We propose for further studies a simple, efficient, seed layer-free and low temperature hydrothermal growth technique to fabricate high quality ZnO nanorods/*p*-GaN heterojunction LED nanodevices. It is also demonstrated that a single short wavelength emission can be shifted to the violet range with Cd-alloying of ZnO used for LED structure.

1. Introduction

The development of efficient short-wavelength light emitting diodes (LEDs) has attracted much attention in the last few years. Near-UV and violet-blue sources can be combined with efficient phosphors for solid-state lighting to replace traditional lamps due to their characteristics of long lifetimes and energy saving [1,2]. There exists an increasing demand for LEDs in automobiles headlights, street lighting, back-lighting for display and so on. Nowadays, InGaN- and GaN-based LEDs are under intense research [3]. However, ZnO is a promising alternative emitting material due to many advantageous properties such as a direct bandgap at 3.37 eV, a large exciton binding energy of 60 meV at room temperature and nanostructuration [4–7]. Heterojunction of *n*-ZnO/*p*-GaN for light emitting devices is one of the best candidates for near-UV LEDs, if we consider a large variety of promising results reported in the literature [4–11]. In particular, the devices based on ZnO-nanorods/*p*-GaN-thin films heterostructures are interesting due to the possibility of improved light extraction from nanorod-based devices. Also, the potential for cost-efficient fabrication of ZnO based devices is very attractive. With ZnO nanotips perpendicularly grown on transparent *p*-GaN-LEDs by metal–organic chemical vapor deposition (MOCVD), the light output power of such LEDs was improved by 1.5–1.7 times compared with conventional ones [8–11]. However, current techniques, such as MOCVD, are applied at elevated temperatures to synthesize high quality ZnO nanorods/nanotips, that may degrade the ohmic contact with *p*-GaN and result in significantly increased forward bias of GaN-LEDs [8]. In addition, the quality of *p*-GaN:Mg will be affected by Mg-dopant activation during the high-temperature process. To avoid these disadvantages, cost-effective, low-temperature electrochemical or aqueous solution methods for growing zinc oxide nanorods on *p*-electrode of GaN-LEDs was recently demonstrated [4–6,12,13]. The effect of different growth regimes, which affect the density of zinc oxide nanorod arrays and respectively the light extraction efficiency, was also experimentally investigated [4,5,12–14]. High-density nanorod arrays were proved to be able to

* Corresponding author at: Laboratoire d'Electrochimie, Chimie des Interfaces et Modélisation pour l'Energie (LECIME) UMR-7575, ENSCP-Chimie Paristech, 11 rue Pierre et Marie Curie, 75231 Paris, cedex 05, France. Tel.: +33 1 55 42 63 83; fax: +33 1 44 27 67 50.
** Corresponding author. Tel.: +33 1 55 42 63 83; fax: +33 1 44 27 67 50.
E-mail addresses: lupan@physics.ucf.edu (O. Lupan), thierry-pauporte@chimie-paristech.fr (T. Pauporté).

0169-4332/$ – see front matter © 2012 Elsevier B.V. All rights reserved.
http://dx.doi.org/10.1016/j.apsusc.2012.07.058

extract much more light out of GaN-based LEDs than lower density nanorod arrays. Directional output behavior of the GaN-based LEDs with hydrothermal synthesis (HT) and electrochemical deposition (ECD) ZnO nanorod arrays was also observed [12–14]. However, in previous papers on HT-ZnO the reported threshold voltage was usually about 10 V [13] and the best experiments gave a threshold voltage of about 5 V [15–17]. In this study, we have investigated the influence of the hydrothermal synthesis versus electrochemical deposition on the optical properties of ZnO/*p*-GaN LEDs.

Hydrothermal synthesis of nano-ZnO is an efficient and green procedure of ZnO nanorod growth on many types of surfaces. Electrochemical deposition (ECD) has become an important technique for fabricating ZnO nanowire-based heterojunctions due to its simplicity, cost-efficiency, large-area deposition and good-quality nanorod arrays [4,18–21]. Hydrothermal and electrochemical are both low temperature solution growth techniques. As was proven before [4–6], an improved heterostructure is expected when GaN is used. ZnO and GaN both have the same wurtzite hexagonal structure, similar lattice parameters, a small in-plane lattice misfit constant (~1.8%),[21] the same stacking sequence (2H) [22], a strong exciton binding energy of 60 meV for ZnO compared to 25 meV for GaN that would favor light emission at room temperature from zinc oxide [4,5,14,23]. Our previous reports on the hydrothermal synthesis technique of ZnO nanorods will serve as a reference for this work [24–26]. In this report, we present the adapted growth conditions, which give the desired ZnO nanorods dimensions on *p*-GaN surface and improved optical quality to achieve high light extraction. The results are compared to our previously reported ECD ZnO-NR/NW layers grown on *p*-GaN. In premiere for hydrothermal synthesis it was demonstrated that a single short wavelength emission can be shifted in the violet range with Cd-alloying of ZnO used for LED structure.

2. Experimental details

The ZnO nanorod arrays on *p*-GaN substrates were grown hydrothermally according to a procedure described elsewhere in our previous papers [24–27]. The *p*-type substrate was a commercial magnesium-doped GaN(0 0 0 1)-oriented layer grown on sapphire with the *c*-axis perpendicular to the substrate (TDI, Inc. Corporation). The GaN layer was ~2.5 μm thick, with a crystal miscut of ~0.59° and a dopant concentration of 4×10^{18} cm^{-3}. Before ZnO deposition, the *p*-GaN(0 0 0 1) substrate was degreased in trichloroethylene at 50 °C for 12 min, subsequently cleaned 6 min in acetone at 52 °C and 8 min in methanol at 22 °C both under ultrasonic and then rinsed with deionized water. Next, the substrate was etched 10 min in concentrated ammonia (27%) at 58 °C, subsequently etched in HCl:H_2O (1:1 vol.) for 15 min to remove any native oxide [5,26–28] and finally rinsed with high purity water (resistivity of 18.2 MΩ cm). This procedure was described in Ref. [5] and was used to clean these *p*-type substrate surfaces.

Zinc sulfate [$Zn(SO_4)\cdot 7H_2O$] and ammonia (NH_4OH) (Fisher Scientific, reagent grade, without further purification) were used for the synthesis of ZnO nanoarchitectures. 0.10–0.15 M $Zn(SO_4)\cdot 7H_2O$ and 2 M ammonia solution NH_4OH (29.6%) were mixed with 100 ml DI–water until complete dissolution at 22 °C and it became colorless [24,27]. Afterwards, the *p*-GaN substrates were placed inside an aqueous solution in a reactor described in our previous papers [24–27]. The set-up was mounted on a hot plate, and the temperature was quickly increased to 95–98 °C and kept constant for 15 min without any stirring. Manipulation and reactions were carried out inside a fume hood. For one set of samples $CdCl_2$ (Alfa Aesar) was added in the bath at 8 μM to perform doping. All samples were exposed to post-deposition annealing at 300 °C in air for 20 min. The as-prepared and thermally processed ZnO NR arrays were characterized by X-ray diffraction (XRD) using a Rigaku 'D/B max' X-ray diffractometer equipped with a monochromatized CuK_α radiation source (λ=1.54178 Å). The operating conditions were 30 mA and 40 kV at a scanning rate of 0.02°/s in the 2θ range from 25° to 130°. Data acquisition was made with the software Data Scan 3.1 and analyzed with Jade 3.1 (from Materials Data Inc.). The morphology was studied using a VEGA TESCAN TS 5130MM scanning electron microscope (SEM). The different characterization techniques confirmed that the nanorod arrays were highly crystalline with regular rods distributed throughout the substrate surface. This morphology is considered to play a major role in nanodevice applications.

The micro-Raman spectra of the ZnO-NW arrays were measured using a Horiba Jobin-Yvon LabRam IR system in a backscattering configuration. The 632.8 nm line of a He–Ne laser was used for off-resonance excitation with less than 4 mW power at the sample. The continuous wave (cw) photoluminescence (PL) was excited by the 325 nm line of a He–Cd laser by Melles Griot. The emitted light was collected by lenses and was analyzed with a double spectrometer providing a spectral resolution better than 0.5 meV. The signal was detected by a photomultiplier working in the photon counting mode. The samples were mounted on the cold station of a LTS-22-C-330 optical cryogenic system. The LED device, integrating the ZnO-NR/*p*-GaN heterostructure, was maintained by a bulldog clip and was biased with a Keitley 2400 source [5]. Its electroluminescence (EL) was collected by an optical fiber connected to a CCD Roper Scientific detector (cooled Pixis 100 camera) coupled with a SpectraPro 2150i monochromator. The monochromator focal lens was 150 mm, grating of 300gr/mm blazed at 500 nm in order to record the emission of the ZnO in the whole near-UV–visible range.

3. Results and discussions

Fig. 1(a) shows a side-view of the close-packed ZnO NRs hydrothermally grown on the (0 0 0 1) *p*-type GaN substrate. Their mean radius is 180 nm and the rods have a flat top. It can be distinguished a heterostructure *n*-ZnO NRs/*p*-GaN/sapphire, which is used in LEDs. Also, in Fig. 1(a) we can observe that the ZnO/GaN interface is smooth and the nanorods are perpendicular to the *p*-GaN layer. A top view of the ZnO nanorod arrays hydrothermally grown on the *p*-type GaN substrate is presented in Fig. 1(b). On the top view, one can observe the hexagonal section of the NRs with a dense morphology. The lateral facets are oriented in the same direction for the various NRs (Fig. 1(b)) and the top aspect is typical of an epitaxial growth with all the NRs having the same in-plane crystallographic orientation [29,30]. No changes in SEM images were observed for the *n*-$Zn_{1-x}Cd_xO$ NRs/*p*-GaN:Mg. The *n*-type ZnO is epitaxially grown directly on the (0 0 0 1) *p*-type GaN:Mg.

The θ/2θ XRD pattern of the heterostructure (*n*-ZnO NRs/*p*-GaN) is dominated by both ZnO and GaN reflection peaks (Fig. 2). Single crystalline GaN film is oriented with the *c*-axis perpendicular to the sapphire substrate. On the enlarged view (Fig. 2(b)), we observe the ZnO(0 0 0 2) diffraction peak on the left-side of GaN(0 0 0 2) reflection. Fig. 2(c) shows the enlarged views of the ZnO(0 0 0 4) peak on the left-side of the GaN(0 0 0 4) reflection. XRD data confirm that GaN and HT-ZnO have the same out-of-plane orientation. The patterns are typical of a perfectly textured ZnO material. The full width at half maximum of (0 0 0 2) peak for ZnO and GaN are the same at 0.07° and close to the apparatus line width. The value is typical of a very high quality well-crystallized heterostructure. The rods are very well-crystallized with a large size (radius measured at about 180 nm, each rod being a single crystal). From XRD (not shown) it was observed a slight lattice deformation/expansion for Cd-ZnO NWs due to these differences in ionic radii ($r(Zn^{2+}) = 0.074$ nm,) by Cd ($r(Cd^{2+}) = 0.095$ nm). The lattice constants for our samples *a* and

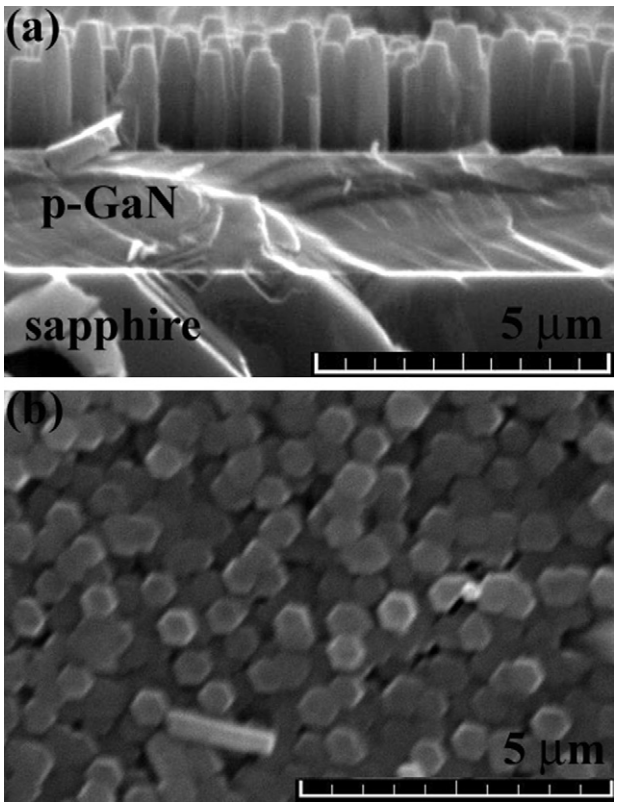

Fig. 1. SEM images: (a) side-view and (b) top-view of epitaxial HT-ZnO nanorods hydrothermally grown on *p*-GaN substrate at 98 °C for 15 min.

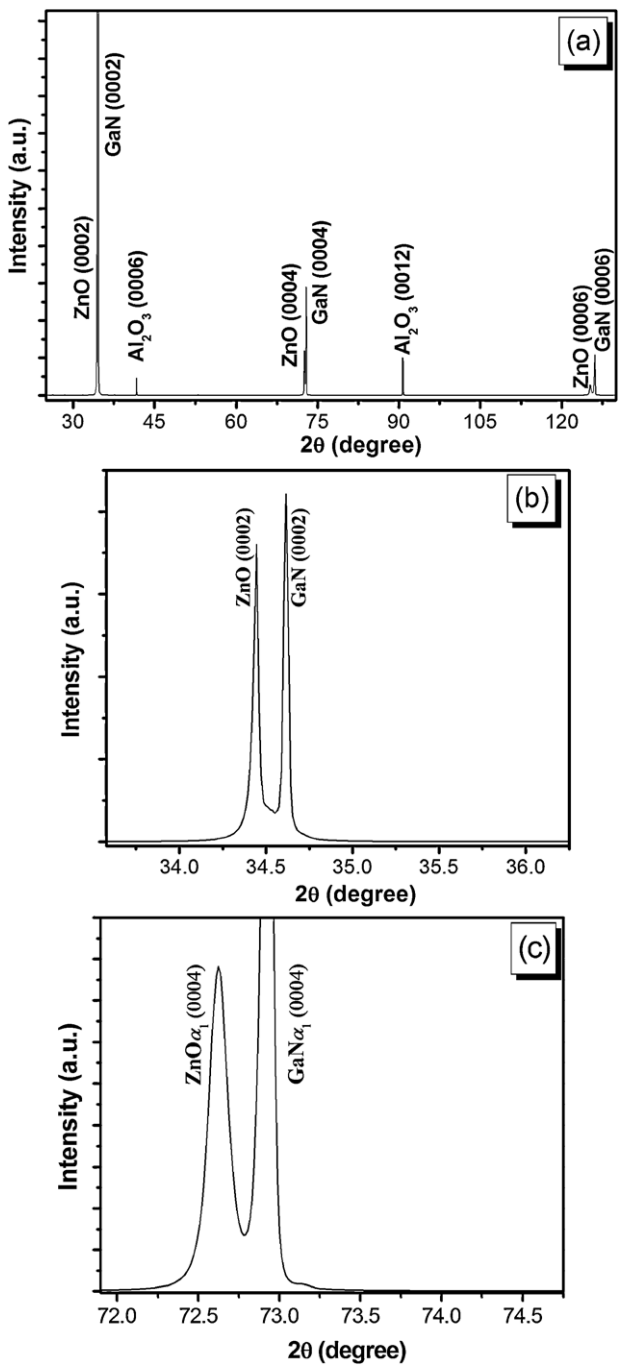

Fig. 2. XRD pattern: (a) of the HT-ZnO-NRs/*p*-GaN/Al_2O_3 (0 0 0 1) structure; (b) enlarged view of the ZnO(0 0 0 2)/GaN(0 0 0 2) region; and (c) enlarged view of the ZnO(0 0 0 4)/GaN(0 0 0 4) region.

c of wurtzite structure ZnO were calculated as reported before [7] and we obtained $a = 3.2506$ Å, $c = 5.2055$ Å for pure ZnO NWs. For concentrations of Cd (8 μM)-doped ZnO NWs, an increase in the lattice parameters *a* and *c* (3.2507 Å and 5.209 Å, respectively) was found. The crystallite size width d_{vol} derived from the Scherrer's formula [7] for all samples was about 350 nm.

The room-temperature micro-Raman spectrum of the heterostructure is indexed with GaN and ZnO emission modes in Fig. 3. The Raman peaks located at 100 cm^{-1} and 439 cm^{-1} are attributed to the ZnO low- and high-E_2 modes, respectively [31–33]. The high-E_2 mode is clearly visible at 439 cm^{-1} with a FWHM of 8 cm^{-1}, while the line-width of the peak corresponding to E_2(low) mode is about 3 cm^{-1}, indicating on high quality HT-ZnO [31].

Fig. 4 compares the photoluminescence (PL) spectra of two samples: the sample #1 hydrothermally grown as presented above and the sample #2 grown by electrochemical deposition in a bath with aqueous solution containing 0.10 mM of $ZnCl_2$ plus 0.1 M KCl as a supporting electrolyte and saturated with O_2. Both samples were grown on *p*-type GaN substrates and subsequently annealed at 300 °C for 20 min in air. The intensity of the near-bandgap UV emission is similar in the compared spectra, while the visible emission is rather different. A weak emission band with the maximum at 2.1 eV which is supposed to be due to the oxygen interstitial [33–36], is observed in the sample #2, while a red band at 1.85 eV is observed in the HT-ZnO sample #1. The presence of oxygen interstitial is highly probable in a sample prepared with an electrolyte saturated with O_2. The emission band at 1.85 eV is an order of magnitude stronger compared to the PL band at 2.1 eV, and it is supposed to be associated with a deep acceptor with the energy level located close to the middle of the bandgap [36]. Unfortunately, it is not possible to establish the microscopic nature of this deep acceptor at this stage.

A detailed analysis of the near-bandgap emission is presented in Fig. 5. The PL spectrum at low temperature is dominated by the donor bound exciton emission (D^0X) at 3.360 eV in both samples, as well as by a donor–acceptor pair recombination band (DA) with phonon LO replica. Note that a neutral donor bound exciton line I_8 related to the Ga impurity with energy close to that observed in our samples was shown to be characteristic for samples grown on GaN substrates, due to the interdiffusion of Ga from the substrate into the ZnO layer [36]. The maximum of the DA band is situated at 3.319 eV and 3.324 eV in the sample #1 and the sample #2, respectively. It is likely that a very shallow donor and a deeper acceptor are involved in this DAP (donor–acceptor pair) transition [37–40]. One can assume that zinc vacancies can play the role of acceptor in these transitions. According to a recent first-principle calculation,

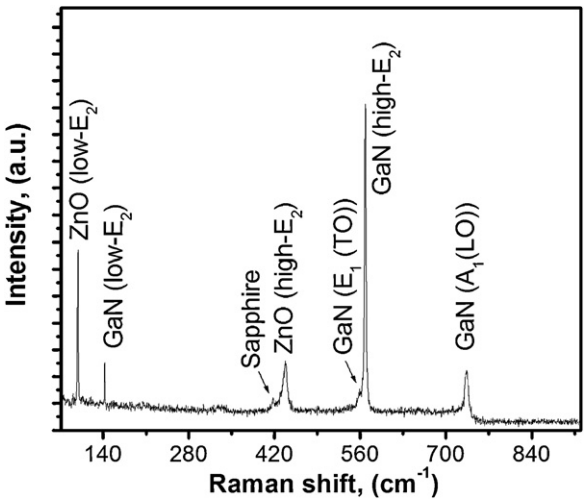

Fig. 3. Room-temperature Raman spectrum of ZnO NRs hydrothermally grown on *p*-GaN thin film/sapphire. Samples were annealed at 300 °C for 20 min.

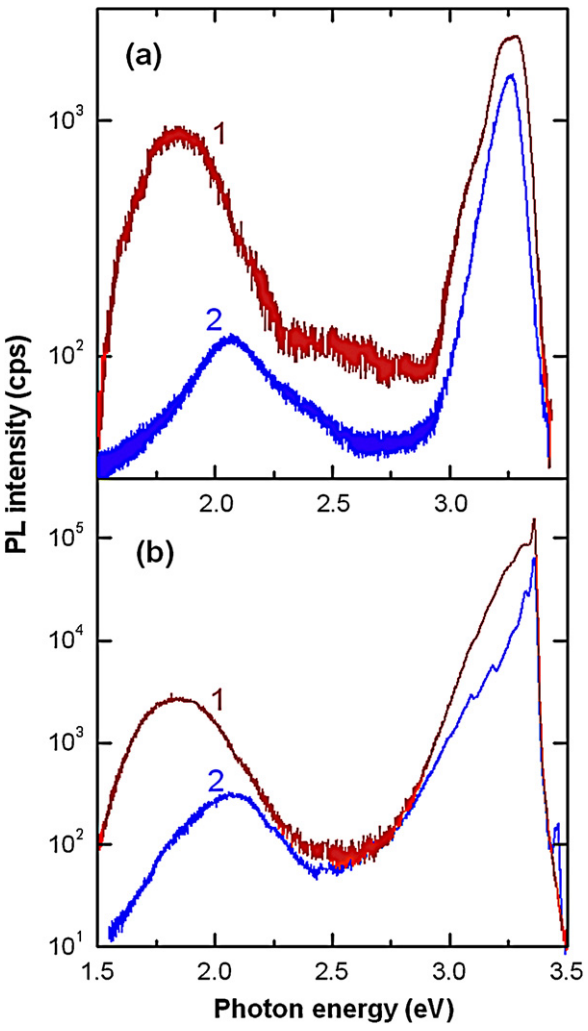

Fig. 4. PL spectra of the hydrothermally grown sample #1 (curve 1) and of a sample grown by electrochemistry (#2, curve 2) measured at: (a) $T = 300$ K; and (b) $T = 10$ K.

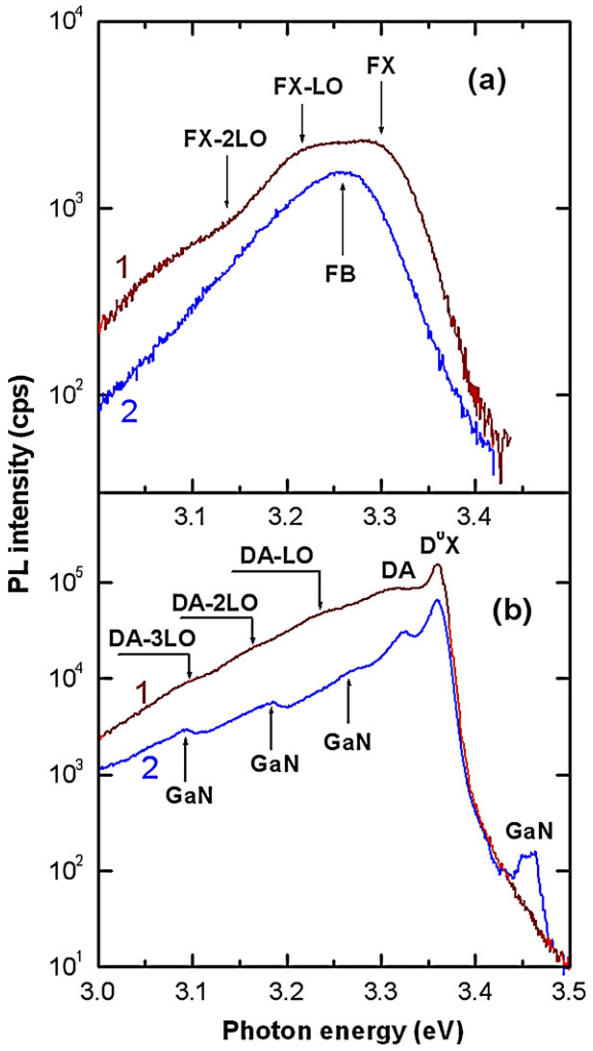

Fig. 5. Near-bandgap PL spectra of the hydrothermally gown sample #1 (curve 1) and of a sample grown by electrochemistry (curve 2) measured at: (a) $T = 300$ K (a) and (b) $T = 10$ K.

the 0/1- acceptor level of the zinc vacancy is situated 0.1–0.2 eV above the valence-band maximum [41]. If one supposes that the same acceptor is present in the compared samples, it means that donors with different activation energies are involved in transitions responsible for the 3.319 eV and 3.324 eV PL bands.

At room temperature, a band (Fig. 5(a)) with the maximum at 3.26 eV is observed in the sample grown by ECD. One can suggest that this band is due to free-to-bound (FB) transitions involving the same acceptor which was involved in DAP transition at low temperatures, while the donors are ionized due to their low activation energy. Taking into account the bandgap of ZnO at room temperature (3.36 eV), one can deduce the energy position of the acceptor level to be located around 100 meV above the valence band, which is compatible with the position of the 0/1-acceptor level of the zinc vacancy as deduced from first-principle calculations. Taking into account this activation energy of the acceptor ($E_A = 100$ meV) and the bandgap of ZnO at low temperatures ($E_g = 3.437$ eV) one can estimate the activation energy of donors involved in the DAP transitions from the relation:

$$E_{D-A} = E_g - E_D - E_A + \left\langle \frac{e^2}{4\pi\varepsilon r} \right\rangle$$

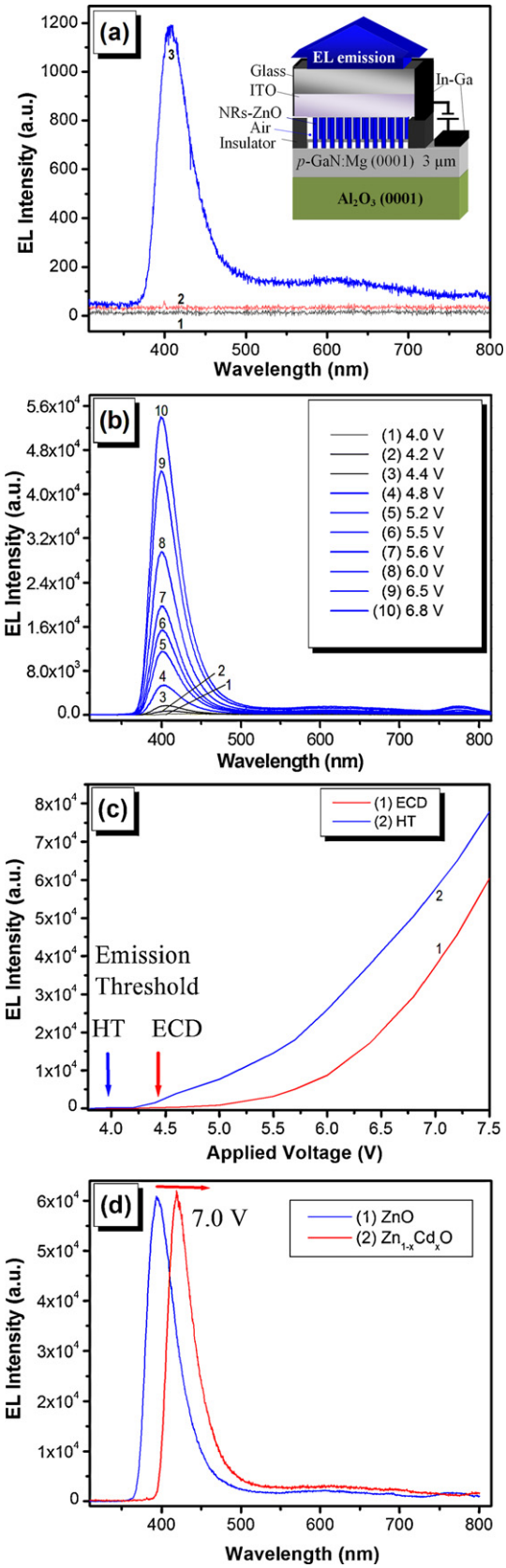

Fig. 6. (a) Electroluminescence spectra of the ITO/ZnO-NRs/*p*-GaN/In-Ga heterojunction light emitting diode (LED) structure under forward bias voltage of 4.3 V. Curves denotes: 1-blank ITO/*p*-GaN, 2–ECD-ZnO/*p*-GaN and 3–HT-ZnO/*p*-GaN. It shows the comparison of EL from the heterojunction LED structure and ITO/GaN/In-Ga structure. Insert shows LED devices structure used in our studies. (b) Relationship between the EL intensity and the forward bias voltage of the fabricated LED structure grown by HT technique. The inset shows voltages applied for each of the investigated curves. (c) Relationship between the electroluminescence intensity and the forward bias voltage of the fabricated LED structure for HT-ZnO and ECD-ZnO. All measurements were performed at 22 °C. (d) Room-temperature electroluminescence spectra of *n*-ZnO/*p*-GaN:Mg and *n*-$Zn_{1-x}Cd_xO$/*p*-GaN:Mg NRs heterostructured LEDs under the forward bias of 7.0 V.

where E_{D-A} is the spectral position of the DA PL band, E_g is the bandgap energy, and E_D and E_A are the binding energies of the donor and the acceptor, respectively. The last term reflects the Coulomb interaction energy. By taking a Coloumb energy of 20 meV [42–44], one can estimate the activation energy of donors involved in the DAP transitions responsible for the 3.319 eV and 3.324 eV PL bands observed at low temperature as being equal to 38 and 33 meV, respectively. Note that several experiments have confirmed the existence of donors in ZnO with energy of 30–40 meV [43,45–49]. It was suggested that these shallow donors contribute to the electrical transport properties of ZnO samples significantly. Some of these donors have been associated with the H impurity in ZnO [43,45–49].

In contrast to the sample grown by ECD, the room temperature near-bandgap PL spectrum of the HT grown sample #1 presents a structured band resulting from the superposition of the band originating from the recombination of free excitons (FX) with the maximum at 3.30 eV with two LO phonon replica.

Note that in addition to the PL bands coming from the ZnO layer, several emission bands coming from the GaN substrates are observed in the low temperature (10 K) PL spectrum of the sample grown by ECD as follows: a weak emission at 3.456 eV is due to the recombination of acceptor bound excitons in the GaN substrate, the band at 3.277 eV is a zero-phonon line of the donor–acceptor pair recombination in the GaN substrate, while the lines at 3.185 eV, and 3.093 eV are the phonon replica with a LO phonon energy of 92 meV characteristic for a GaN crystal with wurtzite structure. No emission from the GaN substrate is observed at room temperature. On the other hand, no emission from the GaN substrate was observed in the sample #1 even at low temperature. This is due to the higher density of the ZnO nanowires in this sample.

The electroluminescence of the LED structure was studied at low bias at room-temperature (RT). For the HT-ZnO based device, a threshold for the UV-EL was detected at a remarkably low forward voltage of about 3.9–4.0 V and the UV-EL signal increased with the applied forward bias. No signal was detected under reverse bias. Fig. 6(a)

presents EL spectra measured at 4.3 V. Curves 1 and 2 are the EL spectra from the blank ITO/GaN and sample #2 (ECD-ZnO/*p*-GaN), without any electro-emissions. Curve 3 shows EL from hydrothermally grown sample #2, which is characterized by a unique emission peak centered at 399 nm and with a FWHM of about 38 nm. The maximum of the EL wavelength is red-shifted compared to the PL emission of ZnO and GaN by about 18 nm and 28 nm, respectively. However, we can observe that the general shape of both ZnO-PL and EL emissions are similar with the presence of a tail in the violet-blue region. Also, it can be concluded from curve 3 of Fig. 6(a) that the emission occurs from the *n*-ZnO/*p*-GaN heterojunction (sample #2–hydrothermal). The violet-blue emission tail could be observed with the naked eye above 5 V. Fig. 6(b) shows a single electroluminescence emission peak which maximum wavelength emission does not shift with the applied voltage. The low emission threshold and strong UV-emission at low voltage are remarkable and demonstrate that the interface between the two semiconductors is of very high quality with a very low density of defects and that the developed hydrothermal technique along with previously reported electrodeposition procedure [4–6] are effective to produce such excellent interfaces.

Fig. 6(c) shows the relationship between the electroluminescence intensity and the forward bias voltage of the LED structure for samples fabricated with HT-ZnO and ECD-ZnO. All measurements were performed at 22 °C.

Fig. 6(d) shows room-temperature electroluminescence spectra of the device structures made from *n*-ZnO/*p*-GaN:Mg and *n*-$Zn_{1-x}Cd_xO$/*p*-GaN:Mg NRs heterostructured LEDs (grown in 8 μM $CdCl_2$ in the bath) under the forward bias of 7.0 V. Room-temperature EL spectra of $Zn_{1-x}Cd_xO$ nanorods are compared with those based of pure ZnO NRs/*p*-GaN LED used as reference (curve 1, Fig. 6(d)). It can be clearly seen a single short wavelength emission shifted in the violet range with Cd-alloying of ZnO. The appearance of the electroluminescence under the forward bias of LED structure and the wavelength shift of up to 24 nm with doping (x) provides insights that the *n*-$Zn_{1-x}Cd_xO$ nanostructures act as the light emitters. It can be concluded that by Cd-doping is possible to tune the emission color by controlling the dopant concentration in $Zn_{1-x}Cd_xO$ NWs. The deviations in the EL and PL spectrum (not shown) could be due to the influence of the heterocontact defects [6,50,51]. We can note that we have also successfully achieved the Cd doping of ZnO by the electrochemical technique using $CdCl_2$ as an additive in the electrodeposition bath [50,51].

The developed hydrothermally grown LED structure possesses improved performances (turn-on voltage ~4 V) compared to those reported in the literature since in most previous works, forward bias beyond 5–10 V had to be applied to observe a significant EL emission. Moreover, in most case visible emissions were found due to defects or doping levels in the emitting material (Mg-deep levels in *p*-GaN, intrinsic defects in ZnO, etc.) [14–16,52–54].

Stability of EL characteristics were investigated in details for both samples and was similar to that we found for ECD-ZnO LED in our previous study [4,50,51].

In this context, we would like to mention that for calculating the light conversion efficiency it is required to determine the number of nanowires well connected to the conductive glass and this was not possible in this experiment. Therefore this research is focused on the comparative studies of the electrodeposition and hydrothermal syntheses through the variation of the threshold values and the shape of the EL bands with the absence of the well-known defects emission in the visible range. More details will be discussed in a forthcoming paper.

4. Conclusions

We report on the successful growth of high quality epitaxial ZnO nanorods on *p*-type GaN layers supported on sapphire by seed layer-free low-temperature solution growth methods. The ZnO NRs were deposited by hydrothermal and low-voltage electrochemical techniques. They were vertically oriented with their *c*-axis perpendicular to the (0 0 0 1) oriented GaN substrate. A comparison of their PL and EL emission properties has been done. The PL spectra were dominated by an UV near-band-edge emission at 381 nm due to exciton recombination. The obtained heterojunctions were used to construct light emitting diode structures. For HT-ZnO, a narrow UV-emission peak, centered at 399 nm, was measured at 22 °C above an applied forward bias of 3.9–4.0 V and no emission was found under reverse bias. The electroluminescence increased rapidly with the applied forward voltage and the observed strong emission was highly stable and reproducible. It was demonstrated that the short wavelength emission could be shifted in the violet range by Cd-alloying of ZnO used for LED structure.

Our results clearly state the remarkable effectiveness of hydrothermally grown and electrodeposited epitaxial ZnO as an active layer in solid-state lighting UV-LED devices.

References

[1] H. Morkoç, S.N. Mohammad, Science 267 (5194) (1995) 51–55.
[2] S. Nakamura, G. Fasol, The Blue Laser Diode: GaN Based Light Emitters and Lasers, Springer, Berlin, 1997.
[3] J.K. Sheu, C.J. Pan, G.C. Chi, IEEE Xplore—Photonics Technology Letters 14 (2002) 450.
[4] O. Lupan, T. Pauporté, B. Viana, Advanced Materials 22 (2010) 3298.
[5] O. Lupan, T. Pauporté, B. Viana, I.M. Tiginyanu, V.V. Ursaki, R. Cortés, ACS Applied Materials & Interfaces 2 (2010) 2083.
[6] O. Lupan, T. Pauporté, T. Le Bahers, B. Viana, I. Ciofini, Advanced Functional Materials 21 (2011) 3564.
[7] O. Lupan, T. Pauporté, L. Chow, B. Viana, F. Pelé, L.K. Ono, B. Roldan Cuenya, H. Heinrich, Applied Surface Science 256 (2010) 1895.
[8] K. Dai, C.B. Soh, S.J. Chua, L. Wang, D. Huang, Journal of Applied Physics 109 (2011) 083110.
[9] M.C. Jeong, B.Y. Oh, M.H. Ham, S.W. Lee, J.M. Myong, Small 3 (2007) 568.
[10] J. Zhong, H. Chen, G. Saraf, Y. Lu, C.K. Choi, J.J. Song, D.M. Mackie, H. Shen, Applied Physics Letters 90 (2007) 203515.
[11] A. Sung Jin, C. Jee Hae, Y. Gyu-Chul, H.P. Gil, Applied Physics Letters 92 (2008) 121108.
[12] K.-K. Kim, S.-D. Lee, H. Kim, J.C. Park, S.-N. Lee, Y. Park, S.-J. Park, S.-W. Kim, Applied Physics Letters 94 (2009) 071118.
[13] S. Dalui, C.C. Lin, H.Y. Lee, C.H. Chao, C.T. Lee, IEEE Xplore—Photonics Technology Letters 22 (2010) 1220.
[14] B. Viana, O. Lupan, T. Pauporté, Journal of Nanophotonics 5 (2011) 051816.
[15] A.M.C. Ng, Y.Y. Xi, Y.F. Hsu, A.B. Djurisic, W.K. Chan, S. Gwo, H.L. Tam, K.W. Cheah, P.W.K. Fong, H.F. Lui, C. Surya, Nanotechnology 20 (2009) 445201.
[16] S. Jha, J.-C. Qian, O. Kutsay, J. Kovac Jr., C.-Y. Luan, J.A. Zapien, W. Zhang, S.-T. Lee, I. Bello, Nanotechnology 22 (2011) 245202.
[17] S. Dalui, C.-C. Lin, H.-Y. Lee, S.-F. Yen, Y.-J. Lee, C.-T. Lee, Journal of the Electrochemical Society 157 (2010) H516–H518.
[18] H. Elbelghiti, T. Pauporté, D. Lincot, Physica Status Solidi (A) 205 (2008) 2360–2364.
[19] O. Lupan, T. Pauporté, B. Viana, Journal of Physical Chemistry C 114 (2010) 14781–14785.
[20] T. Pauporté, G. Bataille, L. Joulaud, J.F. Vermersch, Journal of Physical Chemistry C 114 (2010) 194–202.
[21] T. Pauporté, D. Lincot, Applied Physics Letters 75 (1999) 3817–3820.
[22] P. Kung, M. Razeghi, Opto-Electronics Review 8 (2000) 201.
[23] D.J. Rogers, F.H. Teherani, A. Yasan, K. Minder, P. Kung, M. Razeghi, Applied Physics Letters 88 (2006) 141918.
[24] O. Lupan, L. Chow, G. Chai, B. Roldan, A. Naitabdi, A. Schulte, H. Heinrich, Materials Science and Engineering B 145 (1-3) (2007) 57–66.
[25] D. Polsongkram, P. Chamninok, S. Pukird, L. Chow, O. Lupan, G. Chai, H. Khallaf, S. Park, A. Schulte, Physica B: Condensed Matter 403 (2008) 3713–3717.
[26] O. Lupan, L. Chow, G. Chai, A. Schulte, S. Park, H. Heinrich, Materials Science and Engineering: B 157 (2009) 101–104.
[27] L. Chow, O. Lupan, H. Heinrich, G. Chai, Applied Physics Letters 94 (2009) 163105.
[28] J.J. Uhlrich, L.C. Grabow, M. Mavrikakis, T.F. Kuech, Journal of Electronic Materials 37 (4) (2008) 439–447.
[29] T. Pauporté, D. Lincot, B. Viana, F. Pellé, Applied Physics Letters 89 (2006) 233112.
[30] T. Pauporté, T. Yoshida, R. Cortès, M. Froment, D. Lincot, Journal of Physical Chemistry B 107 (2003) 10077.
[31] O. Lupan, V.V. Ursaki, G. Chai, L. Chow, G.A. Emelchenko, I.M. Tiginyanu, A.N. Gruzintsev, A.N. Redkin, Sensors and Actuators B 144 (2010) 56–66.
[32] G.Y. Chai, L. Chow, O. Lupan, E. Rusu, G.I. Stratan, H. Heinrich, V.V. Ursaki, I.M. Tiginyanu, Solid State Sciences 13 (2011) 1205–1210.
[33] O. Lupan, G.A. Emelchenko, V.V. Ursaki, G. Chai, A.N. Redkin, A.N. Gruzintsev, I.M. Tiginyanu, L. Chow, L.K. Ono, B. Roldan Cuenya, H. Heinrich, E.E. Yakimov, Materials Research Bulletin 45 (2010) 1026–1032.
[34] X.L. Wu, G.G. Siu, C.L. Fu, H.C. Ong, Applied Physics Letters 89 (2001) 2285–2287.
[35] C.H. Ahn, Y.Y. Kim, D.C. Kim, S.K. Mohanta, H.K. Cho, Journal of Applied Physics 105 (2009) 013502.
[36] Ü. Özgür, Ya.I. Alivov, C. Liu, A. Teke, M.A. Reshchikov, S. Doğan, V. Avrutin, S.-J. Cho, H. Morkoç, Journal of Applied Physics 98 (2005) 041301.
[37] B.K. Meyer, J. Sann, S. Lautenschläger, M.R. Wagner, A. Hoffmann, Physical Review B 76 (2007) 184120.
[38] K. Nakahara, H. Takasu, P. Fons, A. Yamada, K. Iwata, K. Matsubara, R. Hunger, S. Niki, Applied Physics Letters 79 (2001) 4139.
[39] V.V. Ursaki, I.M. Tiginyanu, V.V. Zalamai, V.M. Masalov, E.N. Samarov, G.A. Emelchenko, F. Briones, Semiconductor Science and Technology 19 (2004) 851–854.
[40] V.V. Ursaki, I.M. Tiginyanu, V.V. Zalamai, V.M. Masalov, E.N. Samarov, G.A. Emelchenko, F. Briones, Journal of Applied Physics 96 (2004) 1001–1006.
[41] V.V. Ursaki, O.I. Lupan, L. Chow, I.M. Tiginyanu, V.V. Zalamai, Solid State Communications 143 (2007) 437.
[42] M.D. McCluskey, S.J. Jokela, Journal of Applied Physics 106 (2009) 071101.
[43] D.C. Look, Semiconductor Science and Technology 20 (2005) S55–S61.
[44] A. Zeuner, H. Alves, J. Sann, W. Kriegseis, C. Neumann, D.M. Hofmann, B.K. Meyer, A. Hoffmann, U. Haboeck, M. Strassburg, A. Kaschner, Physica Status Solidi (C) 1 (2004) 731–734.

[45] D.M. Hofmann, A. Hofstaetter, F. Leiter, H. Zhou, F. Henecker, B.K. Meyer, S.B. Orlinskii, J. Schmidt, P.G. Baranov, Physical Review Letters 88 (2002) 045504.
[46] D.C. Look, R.L. Jones, J.R. Sizelove, N.G. Garces, N.C. Giles, L.E. Halliburton, Physical Status Solidi A 195 (2003) 171.
[47] Y.M. Strzhemechny, J. Nemergut, P.E. Smith, J. Bae, D.C. Look, L.J. Brillson, Journal of Applied Physics 94 (2003) 4256.
[48] C.H. Seager C H, S.M. Myers, Journal of Applied Physics 94 (2003) 2888.
[49] C.W. Litton, D.C. Reynolds, T.C. Collins (Eds.), Zinc Oxide Materials for Electronic and Optoelectronic Device Applications, John Wiley and Sons, 2011.
[50] O. Lupan, T. Pauporté, Le.T. Bahers, I. Ciofini, B. Viana, Journal of Physical Chemistry C 115 (30) (2011) 14548.
[51] T. Pauporté, O. Lupan, B. Viana, Physica Status Solidi (A) 209 (2) (2012) 359–363.
[52] X.M. Zhang, M.Y. Lu, Y. Zhang, L.J. Chen, Z.L. Wang, Advanced Materials 21 (2009) 2767.
[53] C.H. Chen, S.J. Chang, S.P. Chang, M.J. Li, I.C. Chen, T.J. Husueh, C.L. Hsu, Applied Physics Letters 95 (2009) 223101.
[54] S. Kishwar, K. ul Hasan, N.H. Alvi, P. Klason, M. Willander, Superlattices and Microstructures 49 (2011) 32.